Supporting Information

Super-resolved Traction Force Microscopy (STFM)

Huw Colin-York[1], Dilip Shrestha[1], James H. Felce[1], Dominic Waithe[2], Emad Moeendarbary[3], Simon J Davis[1], Christian Eggeling[1,2,*], and Marco Fritzsche[1,*]

[1]MRC Human Immunology Unit and [2]Wolfson Imaging Centre Oxford, Weatherall Institute of Molecular Medicine, University of Oxford, Headley Way, OX3 9DS Oxford, United Kingdom and [3]Department of Biological Engineering, Massachusetts Institute of Technology, Cambridge, Massachusetts 02142, USA and Department of Mechanical Engineering, University College London, WC1E 7JE London, United Kingdom

S1. Cell culture

RBL-2H3 cells (CRL-2256, ATCC, USA) were cultured at 37°C in 5% CO_2 in MEM (Sigma Aldrich, UK) containing 15% FCS (Sigma Aldrich), 10mM HEPES (Lonza, UK), Penicillin Streptomycin 1% (Sigma Aldrich) and L-glutamine 1% (Sigma Aldrich). 24hrs prior to traction force experiments, adherent cells were treated with 0.05% trypsin (Lonza), faciliting their detachment from the cell culture flask. Cells were then transferred to a rotating chamber to suspend them prior to the experiments.

RBL cell lines stably expressing Lifeact-citrine were generated using a lentiviral transduction strategy. HEK-293T cells were plated in 6-well plates at 3×10^5 cells/ml, 2 ml/well in DMEM (Sigma Aldrich) + 10% FCS (Sigma Aldrich). Cells were incubated at 37°C and 5% CO_2 for 24 h before transfection with 0.5 μg/well each of the lentiviral packaging vectors p8.91 and pMD.G and the relevant pHR-SIN lentiviral expression vector using GeneJuice (Merck Millipore) as per the manufacturer's instructions. 48 h post transfection, the cell supernatant was harvested and filtered using a 0.45 μm Millex-GP syringe filter unit to remove detached HEK-293T cells. 3 ml of this virus-containing medium was added to 1.5×10^6 RBL cells in 3 ml supplemented RPMI medium. After 48 h, cells were moved into 10 ml supplemented MEM and passaged as normal.

S2. Polyacrylamide gel preparation

Polyacrylamide (PAA) gel preparation has been adapted from [1]. Specifically, 40% acrylamide (Sigma Aldrich) and 2% bis-acrylamide (Sigma Aldrich) solutions were combined at final concentrations of 4% and 0.3% respectively, resulting in a gel stiffness of 3kPa. Polymerisation was initiated by adding ammonium persulfate (APS) (Sigma Aldrich) and tetramethylethylenediamine (TEMED)(Sigma Aldrich) at volume ratios of 1:100 and 1:1000, respectively. Once initiated, the gel solution was quickly pipetted between two coverslips, forming a sandwich. Prior to forming the sandwich, the lower coverslip was coated with a high density of fluorescent beads. To achieve a good coverage of fluorescent beads on the coverslip, the glass was first acid cleaned and then

coated with poly-l-lysine 0.01% (Sigma Aldrich) for 10mins. After washing and drying, a solution containing a high concentration of 40 nm red (594/620) fluorescent beads (Invitrogen, UK) was placed onto the coverslip for 10mins, followed by washing and drying. The top coverslip was treated with (3-aminopropyl)trimethoxysilane (APTMS) 0.5% (Sigma Aldrich) followed by treatment with glutaraldehyde 0.5% (Sigma Aldrich) solution. This results in the silanization of the glass surface which forms a covalent link with the polymerising gel, assuring firm attachment of underside of the gel to the coverslip. Once the sandwich was formed, the PAA gel was allowed to polymerise for 30mins at room temperature. Once complete, the top coverslip was peeled off the gel, leaving a thin layer of gel on the activated surface. The PAA gel was then washed extensively in 100x vol/vol PBS and stored at 4°C for no longer than 2 weeks.

S3. Polyacrylamide gel functionalization

To achieve a homogeneous coverage of IgE protein (clone SPE-7, D8406, Sigma Aldrich), the top surface of the PAA gel was initially coated with poly-L-lysine using the bifunctional cross linker suflo-SANPAH (Thermo Fisher Scientific , UK). To achieve this, the gel was first coated with a solution of suflo-SANPAH (2 mg/ml) and then exposed to UV light at a wavelength of 365 nm for 10mins (Stratalinker 2400, Stratagene, USA). This resulted in the covalent attachment of the cross-linker to the gel and left an NHS group for the binding with the free amines on the poly-L-lysine. After UV exposure, the excess cross-linker was washed off three times with 100x vol/vol PBS and the PAA gel placed face down on the drop of poly-L-lysine solution (1 mg/ml) and is allowed to bind overnight. The PAA gel was then washed again with 100x vol/vol PBS before being placed on a drop of IgE solution (10 μg/ml) and incubated overnight.

S4. Confocal and STED imaging

All images were acquired using a Leica SP8-STED inverted microscope (Leica microsystems GMBH, Germany) equipped with a pulsed white-light-laser (80MHz) for fluorescence excitation and a 63x 1.2 water immersion objective, which allowed for high resolution, low aberration imaging at the top surface of the gel at a depth of 20-30 μm (see Figure S1a,b for comparison of water and oil objectives). The microscope was also equipped with an incubation system allowing all measurements to be performed at 37°C in 5% CO_2. The excitation wavelengths used to image the Lifeact-citrine and fluorescent beads were 488 nm and 594 nm, respectively. A continuous-wave 660 nm STED depletion beam and gated detection (gate at 1.5 ns with respect to excitation pulse) was used for all 2-dimensional super resolution STED imaging of the fluorescent beads. Using the described imaging parameters, TFM and STFM was performed sequentially on approximately 30 RBL cells over a number of days and the data presented in Figure 2 is representative of the results acquired.

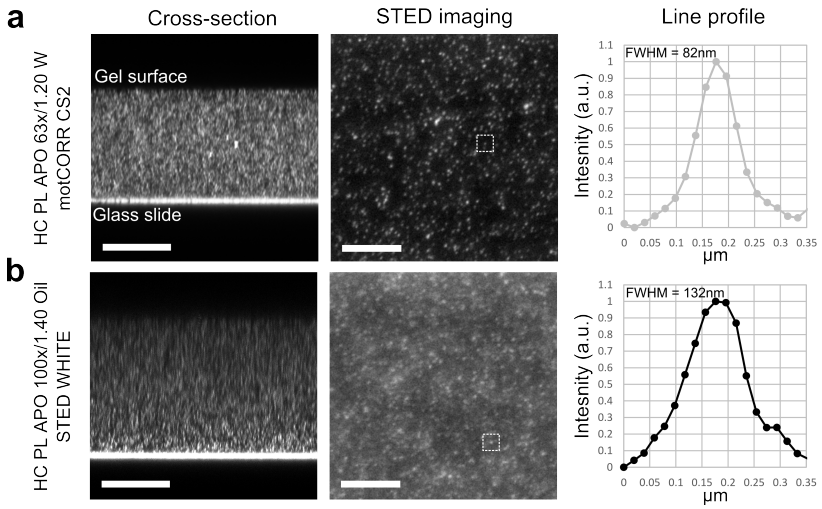

Figure S1: Confocal (left, x-z cross-section, scale bar 20 μm) and STED (middle, x-y image of top gel surface, scale bar 2 μm) of red fluorescent beads (white) in the PAA gel layer on microscope cover glass using **a)** a water and **b)** an oil immersion objective lens. In the x-z cross-section, the cover glass surface is highlighted by a strong continuous signal, while the top surface of the gel is revealed by a vanishing signal. It becomes obvious that the quality of the images becomes worse the deeper one images into the gel, due to optical aberrations, which is less pronounced for the water immersion objective. The right panels depict intensity line profiles through the images of individual beads (dotted squares), highlighting the effective spatial resolution of the STED recordings of 82 and 132 nm, respectively for the the water and oil objective lens.

S5. Bead displacement analysis

Single Particle Tracking (SPT)

Tracking of the fluorescent bead markers necessary to quantify the gel displacement was done using custom written MATLAB routines (MATLAB R2015a, Mathworks, USA). Firstly, a feature finding algorithm was used to establish the location of each marker bead in the first frame of the time-lapse [2]. Next, for each bead, a local region of interest was defined and a 2D Gaussian fit applied, representing a model of each particular bead (Figure S2a). To establish the location of the bead in subsequent frames, the fitted Gaussian was cross-correlated with a wider region of interest (Figure S2b). The maximum value in the cross-correlation corresponds to the likely position of that bead in the given frame. The position of the peak relative to the position of the bead in the previous frame indicates the displacement of that bead and joining these positions provides a track of the displacement. To make this process more robust against selecting the wrong bead, the cross-correlation was multiplied by a 2D Gaussian function with a mean centred on the position of the bead in the previous frame (Figure S2c,d). This serves to bias the cross-correlation to selecting beads that had not moved significantly from the original position. The width of this biasing function allowed for the control of the maximum expected displacement of each bead between frames. Once bead tracks were calculated, the displacement between each frame was interpolated onto a regular mesh required for the traction calculation by Fourier Transform Traction Cytometry (FTTC).

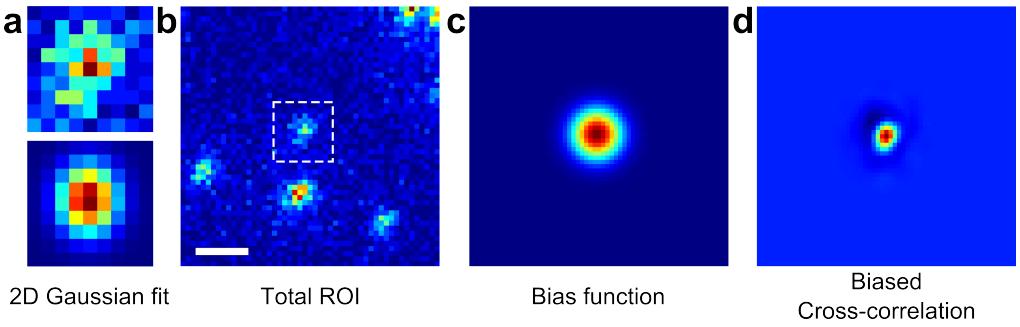

Figure S2: Outline of the bead tracking method. **a)** Zoom in to the image of an individual bead (top) and resulting Gaussian fit to the bead image (bottom). **b)** Larger field-of-view image of the bead shown in a) (dotted square), showing the region of interest (ROI) surrounding the bead. Scale bar 200 nm. **c)** Gaussian bias function, the width of which defines the expected bead displacement. **d)** Cross correlation of the fitted bead image **a)** and the ROI **b)** multiplied by the bias function **c)**. This was performed for each frame of the time-lapse and the peak in the biased cross-correlation calculated, indicating the most likely position of the bead in each frame.

Effect of bead resolution on displacement recovery

As mentioned, an important consideration in TFM is the algorithm chosen to extract the displacements of the beads. To asses the effect of bead resolution on the ability to extract the displacements we extend the simulation procedure to test SPT (described above) and Particle Image Velocimetry (PIV), two image analysis techniques commonly used in TFM. The PIV algorithm used in this work is a MATLAB implementation available at http://www.oceanwave.jp/softwares/mpiv/.

The simulations were conducted by first producing a traction field and the corresponding displacement field (see Figure S3a). The displacement field is then sub-sampled at a density of 15 beads per μm^2. Using the randomly selected bead positions, the sparse vector displacement field is transformed into two fluorescent bead images representing the bead positions before and after the application of the traction. For each bead position we create a point spread function with a confocal (250nm) or STED (40nm) full width at half maximum (FWHM). Noise is added to the simulated images at a level consistent with that observed in the experimental data.

For each pair of images, we employ SPT or PIV to extract the displacements. As can been seen in Figure S3b, when PIV is applied to the STED images it is apparent that displacement recovery and hence the traction recovery better matches the simulation when compared to confocal PIV. In both STED and confocal PIV, a grid size of 500nm was used. Despite the obvious improvement in the reconstruction the DTM fails to represent this (see Table S1). This is due to the DTMs reliance on the overall traction magnitude to determine the success of reconstruction. In the confocal and STED PIV case, the magnitudes of tractions are similar, but the spatial distribution is much improved using STED. To quantify this, we introduce a new metric which is the normalised least square error (NLS). This metric, which assesses the difference in the two recoveries across the field of view, now shows the difference, with STED-PIV scoring lower than confocal-PIV (see Table S1). Note, the optimum NLS would be zero for a perfect recovery.

For SPT, it is clear that in the confocal bead images the level of bead crowding prevents their localisation and tracking (see Figure S3a). However, when STED imaging is used the increase in resolution allows reliable tracking and calculation of the traction field. Visual inspection shows a good agreement with the simulation, and quantification using the NLS shows a very similar level of traction recovery to that shown by PIV for the STED images.

These simulations demonstrate that independent of the chosen image analysis al-

gorithm, the increase in resolution made possible by STED microscopy improves the traction recovery.

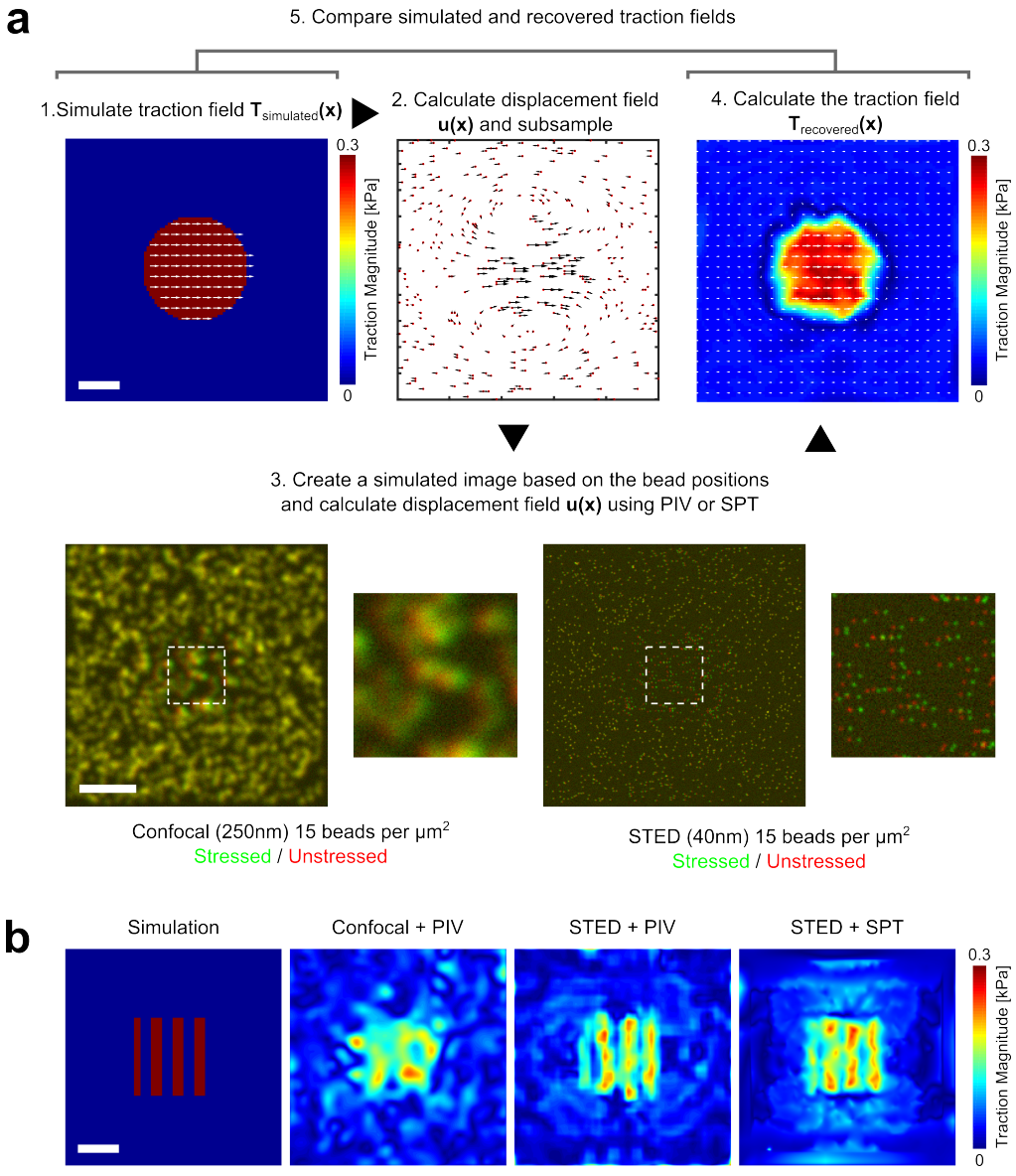

Figure S3: Outline of the simulation process. a) A traction field $T_{simulated}(x)$ is simulated and the corresponding displacement field u(x) calculated (heat map; high traction magnitude warm colours, low traction magnitudes cold colours, white arrows: traction direction). The displacement field is then sub-sampled at 15 beads per μm^2 (red dots: bead positions, black arrows: bead displacements). A pair of fluorescent bead images (stressed-green and unstressed-red) are simulated using the random bead positions and displacements. Bead positions are replaced with PSFs at resolutions corresponding to confocal (250nm) and STED (40nm) (inset: zoom in of boxed region). PIV and SPT are used to extract the bead displacements which are then transformed into the recovered traction field $T_{recovered}(x)$ and the simulation and recovery are compared by the Deviation of Traction Magnitude (DTM) and the Normalised Least Square Error (NLS). Scale bar 2 μm. b) Simulation and traction recovery for a 1 μm wavelength periodic traction pattern (0 - 0.3 kPa) using PIV (confocal and STED) and SPT (STED only). Scale bar 2 μm.

	PIV		SPT	
	Confocal	STED	Confocal	STED
DTM	-0.22 ± 0.02	-0.23 ± 0.01	n/a	-0.18 ± 0.05
NLS	0.48 ± 0.08	0.25 ± 0.01	n/a	0.27 ± 0.04

Table S1: Quantification of the difference in traction recovery using PIV and SPT in combination with confocal and STED imaging. Traction recovery is compared using the Deviation of Traction Magnitude (DTM) and the Normalised Least Square Error (NLS). Note that for PIV the DTM cannot detect the spatially more accurate force field in the case of STED compared to confocal, and we therefore employ the method of the normalized least-squares error to compare the results upon SPT and PIV reconstruction. Also note that SPT is not applicable in the case of confocal recordings due to overlapping PSFs of the imaged beads.

S6. Traction force microscopy (TFM)

Fourier Transform Traction Cytometry

By measuring the lateral displacements of fluorescent beads placed within an elastic gel, TFM allows any tangential forces applied to the gel to be recovered. Mathematically, the gel is defined as an elastic half-space, meaning it is considered to be infinite in all three spatial dimensions [3]. In practice, the gel is of finite thickness and is chemically attached to a cover-slip such that it can be imaged from below. For the half-space assumption to hold, the gel must be sufficiently thick such that any forces applied to the upper surface of the gel are not influenced by the fixed lower surface at the cover-slip. In practice, this means the gel can be no thinner than 20-30 μm and all displacements must be kept below 1 μm [4]. It is also assumed that the direction of forces are limited to the plane of the gel and forces normal to the gel are considered negligible. By imaging the beads before and after a force has been applied, the displacement of each bead can be extracted, providing a displacement field, $\mathbf{u}(\mathbf{x})$, across the extent (two-dimensional space $\mathbf{x}$) of the substrate-cell interface. The traction field, $\mathbf{T}(\mathbf{x})$, and displacement field, $\mathbf{u}(\mathbf{x})$, are related via a convolution with the so called Green's function, $\mathbb{G}$ (Equation 1 and 2). The Green's function is a tensor which maps the traction field to the spatial distribution of the displacements and is dependent on the elastic modulus, E, and the poisson ratio ν (assumed to be 0.5) of the elastic medium [4].

$$\mathbf{u}(\mathbf{x}) = (\mathbb{G} * \mathbf{T})(\mathbf{x}) \tag{1}$$

$$\mathbb{G}(\mathbf{x}) = \frac{1+\nu}{\pi E}\frac{1}{|\mathbf{x}|^3}\begin{pmatrix} (1-\nu)|\mathbf{x}|^2+\nu x_1^2 & \nu x_1 x_2 \\ \nu x_1 x_2 & (1-\nu)|\mathbf{x}|^2+\nu x_2^2 \end{pmatrix} \text{ where, } |\mathbf{x}| = \sqrt{x_1^2+x_2^2} \tag{2}$$

The convolution in Equation 1 can be simplified to a product by applying a Fourier transform to both the traction field and Green's function (denoted by the hat symbol in Equation 3 and 4), which now depend on the spatial wave vector, $\mathbf{k}$ [10]. Equation 1 and 3 represent the forward problem; determining the displacement field from the traction field. In the case of TFM, the problem of interest is the inverse, where the traction field must be calculated from the experimentally measured displacement field. Unfortunately, this cannot simply be achieved by inversion of Equation 3 as the problem is said to be ill-posed [5]. In this case, we define an ill-posed problem as one whose solution is sensitive to noise in the initial conditions. This can be understood by considering the forward problem as a smoothing operation; any traction field applied to the elastic medium results in a smooth displacement field. The experimentally measured displacement field is likely to contain high frequency noise resulting from errors in recording the bead positions, which in the case of simple inversion (Equation 5), will result in a highly

divergent traction field. This is a well known property common to inverse problems and can be resolved by introducing a technique known as regularisation [11].

$$\hat{\mathbf{u}}(\mathbf{k}) = \hat{\mathbb{G}}(\mathbf{k})\hat{\mathbf{T}}(\mathbf{k}) \tag{3}$$

$$\hat{\mathbb{G}}(\mathbf{k}) = \frac{1+\nu}{\pi E}\frac{1}{|\mathbf{k}|^3}\begin{pmatrix} (1-\nu)|\mathbf{k}|^2+\nu k_2^2 & -\nu k_1 k_2 \\ -\nu k_1 k_2 & (1-\nu)|\mathbf{k}|^2+\nu k_1^2 \end{pmatrix} \text{ where, } |\mathbf{k}| = \sqrt{k_1^2+k_2^2} \tag{4}$$

$$\hat{\mathbf{T}}(\mathbf{k}) = \hat{\mathbb{G}}(\mathbf{k})^{-1}\hat{\mathbf{u}}(\mathbf{k}) \tag{5}$$

Regularisation

In the case of simple inversion, the inverse problem is solved for $\hat{\mathbf{T}}$ by minimising the residual norm $\left\|\hat{\mathbb{G}}\hat{\mathbf{T}} - \hat{\mathbf{u}}\right\|^2$. However, as discussed, this will result in an unsatisfactory solution in the presence of experimental noise in the displacement field. Instead, the minimisation condition is modified to include a regularisation term in a technique known as Tikhonov regularisation [6]. The minimisation condition is now modified in such a way that we constrain the value of the solution norm $\left\|\hat{\mathbf{T}}_\lambda\right\|^2$, effectively filtering the high frequency noise and producing a smooth solution (Equation 6). The degree of smoothing is determined by the regularisation parameter, λ.

$$min\left\{\left\|\hat{\mathbb{G}}\hat{\mathbf{T}}_\lambda - \hat{\mathbf{u}}\right\|^2 + \lambda^2\left\|\hat{\mathbf{T}}_\lambda\right\|^2\right\} \tag{6}$$

The expression to be minimised can be solved for $\hat{\mathbf{T}}_\lambda$ for varying values of λ using the following explicit solution, which is the regularised version of Equation 5, in which $\hat{\mathbb{G}}^T$ represents the matrix transpose of $\hat{\mathbb{G}}$ and I is the identity matrix [12]:

$$\hat{\mathbf{T}}_\lambda = (\hat{\mathbb{G}}^T\hat{\mathbb{G}} + \lambda^2 I)^{-1}\hat{\mathbb{G}}^T\hat{\mathbf{u}} \tag{7}$$

The above regularisation scheme allows for a suitable solution to be found in the presence of a noise corrupted displacement field. Using this scheme presents the problem of choosing the correct regularisation parameter, λ. If λ is too small, the solution will be dominated by an overestimation of the noise. On the other hand, if λ is too large the solution will be over-smoothed and the traction field will not be representative of the data. In order to balance these two outcomes, a curve is plotted of the residual norm, $\left\|\hat{\mathbb{G}}\hat{\mathbf{T}}_\lambda - \hat{\mathbf{u}}\right\|$, and the solution norm, $\left\|\hat{\mathbf{T}}_\lambda\right\|$, for varying degrees of regularisation (Figure S4b). This curve typically has a characteristic L-shape, and hence this selection method is known as the L-curve criterion [7]. The corner of the curve represents the optimum balance between fitting the data (lowest residual norm), and constraining the solution (lowest solution norm). In both the simulations and RBL cell experiments, the L-curve is used to select the optimum value for λ. In addition to this, the simulations conducted in Figure 2d,e were repeated 50 times at each condition, ensuring a reliable relationship between the sampling density and the ability to resolve tractions.

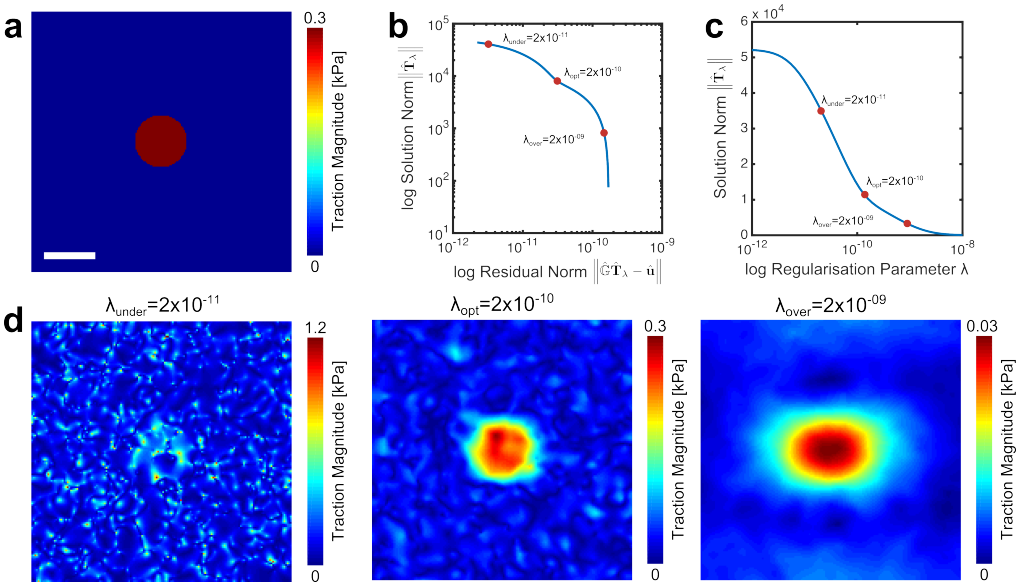

Figure S4: **a)** Simulated circular traction field. Scale bar 2 μm. **b)** Residual norm plotted against the solution norm for a range of regularisation parameters, λ, for the recovery of the simulated traction field. The traction recovery for the three degrees of regularisation indicated along the line are shown in **d)**. **c)** Solution norm for each value of the regularisation parameters. **d)** Recovery of the traction field for each value of the highlighted regularisation parameter: $\lambda = 2 \times 10^{-11}$ (left) shows under-regularisation, over fitting the noise in the data. $\lambda = 2 \times 10^{-09}$ (right) shows over-regularisation, underestimating the traction magnitude. $\lambda = 2 \times 10^{-10}$ (middle), shows the correct degree of regularisation, showing good agreement between the recovery and simulation.

S7. Actin-Gel correlation analysis

To establish the correlation in the direction of actin flow and the displacement of the beads, it was first necessary to quantify the motion of actin within the RBL cell. This was achieved using an optical flow algorithm implemented in MATLAB adapted from [16]. Optical flow is a commonly used technique in computer vision to establish the movement of objects between video frames. By comparing the pixel intensity distribution before and after the movement during a typical STFM recording, the shift or flow between frames is quantified, yielding a pixel-wise vector field of displacements within the fluorescent actin distribution. To gain an understanding of how the gel was moving with the respect to actin, we calculated a point-wise dot product of each gel displacement vector with the actin flow vector, producing a correlation of the two vector fields across the field of view.

Supplementary Movies

Movie S1 - Representative large field-of-view confocal time-lapse movie of an RBL cell expressing Lifeact-citrine (green) spreading on an IgE coated 3 kPa PAA gel loaded with 40 nm red fluorescent beads (red) at a low density (0.4 μm^{-2}). The beads are seen to move beneath the cell, indicating that forces are being transferred by the cell to the gel. Scale bar 10 μm. Frame rate 0.2 s^{-1}. Total acquisition time 200 s.

Movie S2 - Representative close-up confocal time-lapse movie of a RBL cell expressing Lifeact-citrine (green) spreading on an IgE coated 3 kPa PAA gel loaded with 40 nm red fluorescent beads (red) at a low density (0.4 μm^{-2}). Again, the beads are seen to move beneath the cell, indicating that forces are being transferred by the cell to the gel. Scale bar 2 μm. Frame rate 0.2 s^{-1}. Total acquisition time 120 s.

Movie S3 - Equivalent time-lapse movie to that shown in Supplementary Movie S2, this time imaged with STED microscopy in the case of the beads. Scale bar 2 μm. Frame rate 0.05 s^{-1}. Total acquisition time 120 s.

Movie S4 - Representative close-up confocal time-lapse movie of a RBL cell expressing Lifeact-citrine (green) spreading on an IgE coated 3 kPa PAA gel loaded with 40 nm red fluorescent beads (red) at a high bead density (2.2 μm^{-2}). A significant number of beads are seen to overlap, preventing their reliable tracking. Scale bar 2 μm. Frame rate 0.06 s^{-1}. Total acquisition time 48 s.

Movie S5 - Equivalent time-lapse movie to that shown in Supplementary Movie S4, this time imaged with STED microscopy in the case of the beads. The improved spatial resolution made possible using STED now means that all beads in the field of view are trackable. Scale bar 2 μm. Frame rate 0.05 s^{-1}. Total acquisition time 120 s.

References

[1] Tse, J. R. & Engler, A. J., Curr Protoc Cell Biol, **2010**, Chapter 10.

[2] Pelletier, V., and Gal, N., and Fournier, P., and Kilfoil, M., Phys. Rev. Lett., **2010**, 102.188303.

[3] Landau, L., and Lifshitz, E., Course of Theoretical Physics: Theory of Elasticity vol. 7, **1986**, Pergamon Press, Oxford.

[4] Plotnikov, S., Sabass, B., and Schwarz, U., and Waterman, C., Quantitative Imaging in Cell Biology, Vol 123. Methods Cell Biol., **2010**, 367–394.

[5] Engl, H., **1996**, Kluwer Academic Publishers.

[6] Tikhonov, A., Soviet Math. Dokl., **1963**, 5, 1035/1038.

[7] Hansen, P., Invited chapter in Computational Inverse Problems in Electrocardiology, **1999**, 119-142.